Self-Assembly of [*n*]Rotaxanes Bearing Dendritic Stoppers[⊥]

David B. Amabilino,[†] Peter R. Ashton,[†] Vincenzo Balzani,[‡] Christopher L. Brown,[†] Alberto Credi,[‡] Jean M. J. Fréchet,[§] Jeffrey W. Leon,[§] Françisco M. Raymo,[†] Neil Spencer,[†] J. Fraser Stoddart,*[,†] and Margherita Venturi[‡]

Contribution from The School of Chemistry, The University of Birmingham, Edgbaston, Birmingham B15 2TT, UK, Department of Chemistry, Baker Laboratory, Cornell University, Ithaca, New York 14853-1301, and Dipartimento di Chimica "G. Ciamician" dell'Università, via Selmi 2, I-40126 Bologna, Italy

Received June 24, 1996[⊗]

Abstract: We have developed a synthetic approach to the self-assembly of [2]-, [3]-, and [4]rotaxanes, incorporating bis-*p*-phenylene-34-crown-10 as the ring component(s) surrounding bipyridinium-based dumbbell-shaped components bearing dendritic stoppers at both ends. As a result of the hydrophobic dendritic framework, these [*n*]rotaxanes are soluble in a wide range of organic solvents, despite the polycationic natures of their bipyridinium-based backbones. In all cases, they could be purified by means of column chromatography employing relatively low polar eluants. The *molecular shuttling* action of the [2]rotaxane containing two bipyridinium units on the rod portion of the dumbbell-shaped component has been investigated by variable-temperature ^{1}H-NMR spectroscopy in a range of solvents [$CDCl_3$, CD_2Cl_2, THF-d_8, and $(CD_3)_2CO$] for the first time. This investigation reveals a marked dependence of the rate of the *shuttling* process upon the polarity of the media. On going from $CDCl_3$ to $(CD_3)_2CO$, the rate constant increases from *ca.* 200 to 33000 times per second. Molecular dynamics simulations, performed in $CHCl_3$ and Me_2CO on the [2]rotaxane, suggest that significant conformational changes occur upon changing the polarity of the medium resulting in both steric and electronic hindrance of the *shuttling* process in $CHCl_3$. Three-dimensional representations, as well as the approximate sizes—*i.e.* overall lengths and molecular volumes which range from 3 to 6 nm and from 4 to 6 nm^3, respectively—of these molecular compounds, were obtained by means of molecular modeling studies. Thus, these nanometer-scale dendritic rotaxanes resemble naturally-occurring chemical systems incorporating an active component, in so far as the rotaxane-like core with its distinctive recognition features is surrounded by a molecular shell in the form of the dendritic framework.

Introduction

In previous papers, we have reported[1] on the self-assembly[2] of [*n*]rotaxanes[3] incorporating π-electron-deficient dumbbell-shaped components encircled by hydroquinone-based macrocyclic polyethers. Noncovalent bonding interactions, such as (i) $\pi-\pi$ stacking between the complementary aromatic units as well as (ii) hydrogen bonding between the acidic hydrogen atoms in the α-positions with respect to the nitrogen atoms on the bipyridinium units and the polyether oxygen atoms are the main driving forces in these self-assembly processes. These results suggested strongly the possibility of constructing nanoscale[4] molecular compounds possessing device-like properties[5] by combining the convergent approach to dendrimers[6] with our synthetic methodology to self-assembling rotaxanes. Upon combination in solution of a preformed macrocyclic component with an appropriate rod-like derivative, a pseudorotaxane-like complex—the core—self-assembles spontaneously. Subsequent covalent attachment of bulky dendritic stoppers to the core

[⊥] Molecular Meccano, Part 13: for Part 12, see: Asakawa, M.; Ashton, P. R.; Ballardini, R.; Balzani, V.; Bělohradský, M.; Gandolfi, M. T.; Kocian, O.; Prodi, L.; Raymo, F. M.; Stoddart, J. F.; Venturi, M. *J. Am. Chem. Soc.* In press.

[†] University of Birmingham.

[§] Cornell University.

[‡] University of Bologna.

[⊗] Abstract published in *Advance ACS Abstracts,* November 1, 1996.

(1) (a) Ashton, P. R.; Ballardini, R.; Balzani, V.; Bělohradský, M.; Gandolfi, M. T.; Philp, D.; Prodi, L.; Raymo, F. M.; Reddington, M. V.; Spencer, N.; Stoddart, J. F.; Venturi, M.; Williams, D. J. *J. Am. Chem. Soc.* **1996**, *118*, 4931−4951. (b) Asakawa, M.; Ashton, P. R.; Ballardini, R.; Balzani, V.; Bělohradský, M.; Gandolfi, M. T.; Kocian, O.; Prodi, L.; Raymo, F. M.; Stoddart, J. F.; Venturi, M. *J. Am. Chem. Soc.* In press.

(2) (a) Lindsey, J. S. *New J. Chem.* **1991**, *15*, 153−180. (b) Whitesides, G. M.; Mathias, J. P.; Seto, C. T. *Science* **1991**, *254*, 1312−1319. (c) Whitesides, G. M.; Simanek, E. E.; Mathias, J. P.; Seto, C. T.; Chin, D. N.; Mammen, M.; Gordon, D. M. *Acc. Chem. Res.* **1995**, *25*, 37−44. (d) Lawrence, D. S.; Jiang, T.; Levett, M. *Chem. Rev.* **1995**, *95*, 2229−2260. (e) Raymo, F. M.; Stoddart, J. F. *Curr. Op. Coll. Interface Sci.* **1996**, *1*, 116−126. (f) Philp, D.; Stoddart J. F. *Angew. Chem., Int. Ed. Engl.* **1996**, *35*, 1154−1196.

(3) (a) Dietrich-Buchecker, C. O.; Sauvage J.-P. *Bioorg. Chem. Front.* **1991**, *2*, 195−248. (b) Chambron, J.-C.; Dietrich-Buchecker, C. O.; Sauvage, J.-P. *Top. Curr. Chem.* **1993**, *165*, 131−162. (c) Gibson, H. W.; Marand, H. *Adv. Mater.* **1993**, *5*, 11−21. (d) Gibson, H. W.; Bheda, M. C.; Engen., P. T. *Prog. Polym. Sci.* **1994**, *19*, 843−945. (e) Amabilino, D. B.; Stoddart, J. F. *Chem. Rev.* **1995**, *95*, 2725−2828. (f) Bělohradský, M.; Raymo, F. M.; Stoddart, J. F. *Collect. Czech. Chem. Commun.* **1996**, *61*, 1−43.

(4) (a) Ozin, G. A. *Adv. Mater.* **1992**, *4*, 612−649. (b) Merkle, R. C. *Nanotechnology* **1993**, *4*, 86−90. (c) Mann, S. *Science* **1993**, *365*, 499−505. (d) Wibur, J. L.; Kumar, A.; Kim, E.; Whitesides, G. M. *Adv. Mater.* **1994**, *6*, 600−604. (e) Drexler, K. E. *Annu. Rev. Biophys. Biomol. Struct.* **1994**, *23*, 377−405. (f) Kumar, A.; Abbot, N. L.; Kim, E.; Biebuyck, A.; Whitesides, G. M. *Acc. Chem. Res.* **1995**, *28*, 219−226. (g) Bowes, C. L.; Ozin, G. A. *Adv. Mater.* **1996**, *8*, 13−28.

(5) (a) Lehn, J.-M. *Angew. Chem., Int. Ed. Engl.* **1990**, *29*, 1304−1319. (b) Balzani, V.; Scandola, F. *Supramolecular Photochemistry,* Horwood: Chichester, 1991, Chapter 12. (c) Bissell, R. A.; de Silva, A. P.; Gunaratne, H.; Lynch, P. L. M.; Maguire, G. E. M.; Sandanayake, K. R. A. S. *Chem. Soc. Rev.* **1992**, *21*, 187−195. (d) Lehn, J.-M. *Science* **1993**, *260*, 1762−1763. (e) Fabbrizzi, L.; Poggi, A. *Chem. Soc. Rev.* **1995**, *24*, 197−202. (f) Beer, P. D. *Chem. Commun.* **1996**, 689−696.

(6) (a) Tomalia, D. A.; Naylor, A. M.; Goddard, W. A., III *Angew. Chem., Int. Ed. Engl.* **1990**, *29*, 138−17. (b) Kim, Y. H. *Adv. Mater.* **1992**, *4*, 764−766. (c) Newkome, G. R.; Moorefield, C. N.; Baker, G. R. *Aldrichim. Acta* **1992**, *25*, 31−38. (d) Mekelburger, H. B.; Jaworek, W.; Vögtle, F. *Angew. Chem., Int. Ed. Engl.* **1992**, *31*, 1571−1576. (e) van der Made, A. W.; van Leeuwen, P. W. N. M.; de Wielde, J. C.; Brandes, R. *Adv. Mater.* **1993**, *5*, 466−468. (f) Tomalia, D. A.; Durst, H. D. *Top. Curr. Chem.* **1993**, *165*, 193−313. (g) Tomalia, D. A. *Adv. Mater.* **1994**, *6*, 529−539. (h) Rajca, A. *Adv. Mater.* **1994**, *6*, 605−607. (i) Issberner, J.; Moors, R.; Vögtle, F. *Angew. Chem., Int. Ed. Engl.* **1994**, *33*, 2413−2420. (j) Fréchet, J. M. J. *Science* **1994**, *263*, 1710−1715.

S0002-7863(96)02113-0 CCC: $12.00

Scheme 1

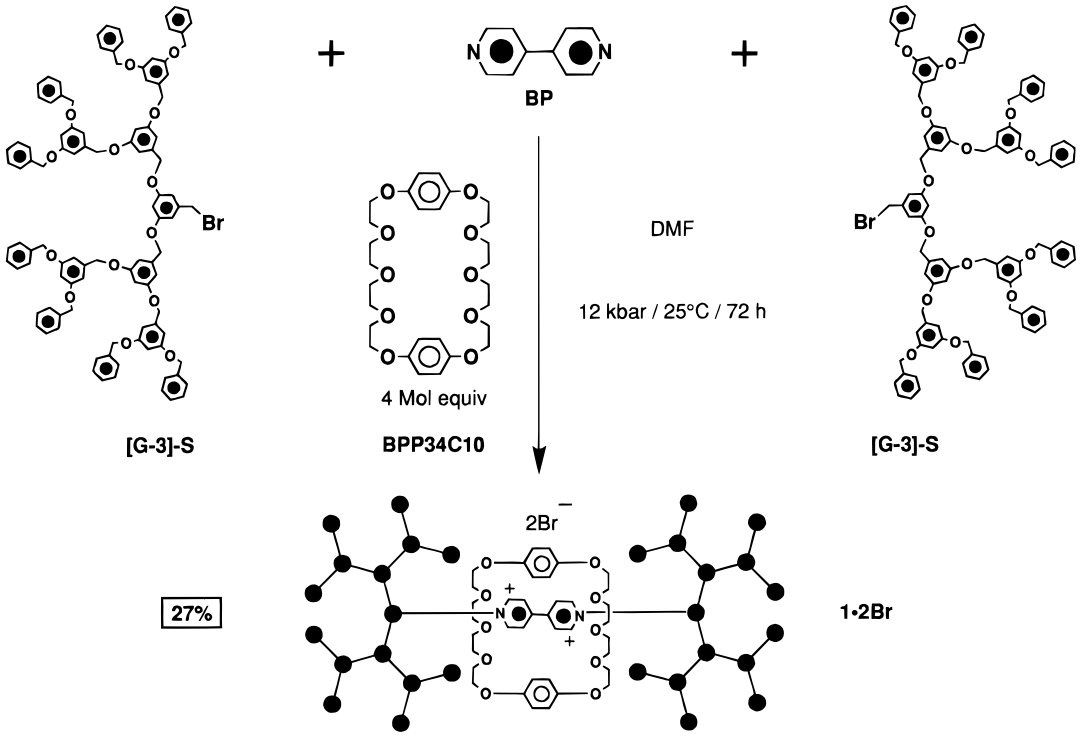

affords a rotaxane incorporating a dumbbell-shaped component bearing dendritic stoppers—*i.e.* a two-directional dendrimer.[7] The multibranched stopper groups are expected to influence (i) the solubility of the rotaxane, (ii) the dynamic processes involving the *shuttling* of the macrocyclic components along the dumbbell-shaped component, as well as (iii) the photochemical and electrochemical properties.

Results and Discussion

Synthesis.[8] A range of [2]-, [3]-, and [4]rotaxanes incorporating dendritic stoppers, the cartoon representation of which is illustrated in Figure 1, were self-assembled by employing a so-called threading[1] approach. The threading of a preformed macrocycle on to a suitable rod-like compound affords a pseudorotaxane-like complex. Subsequent covalent linkage of two dendritic stoppers at both ends of the rod provides a mechanical trap for the macrocyclic component, yielding a rotaxane. Scheme 1 illustrates the self-assembly of the [2]rotaxane **1·2Br** incorporating one **BPP34C10** macrocyclic component and one bipyridinium recognition site located within its dumbbell-shaped component. Reaction of bipyridine **BP** with the generation-three stopper **[G-3]-S** in the presence of four molar equivalents of **BPP34C10** in DMF under ultrahigh pressure conditions at 25 °C during 72 h afforded the [2]rotaxane **1·2Br** in a yield of 27%. Interestingly, as a result of the dendritic shell surrounding the rotaxane core, purification of the dicationic [2]rotaxane **1·2Br** was achieved by column chromatography (SiO_2, CH_2Cl_2/EtOH, 9.5:0.5) employing a relatively low polarity eluant. On the contrary, highly polar eluants are required[1] in order to purify the analogous rotaxanes bearing tetraarylmethane-based stoppers. Furthermore, high solubilities in a range of organic solvents are achieved, despite the fact that relatively hard bromide counterions are employed.

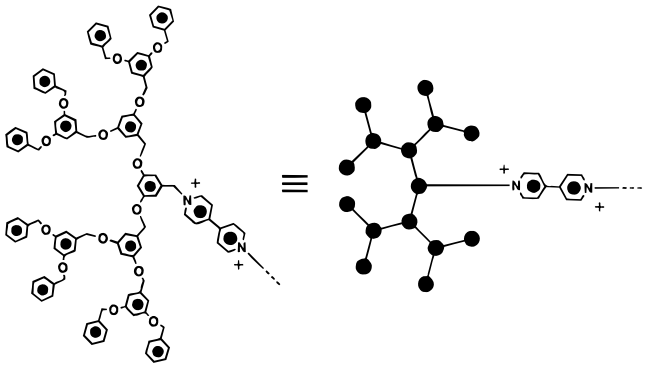

Figure 1. Cartoon representation employed to illustrate the rotaxanes incorporating dendritic stoppers.

By increasing the number of bipyridinium recognition sites incorporated within the dumbbell-shaped component, higher order rotaxanes were self-assembled by employing the same synthetic procedure. Reaction (Scheme 2) of the bis(hexafluorophosphate) salt **[BPYPYXY][PF$_6$]$_2$** with the stopper **[G-3]-S** in the presence of eight molar equivalents of **BPP34C10** in DMF under a pressure of 12 kbar at 25 °C during 72 h afforded the [3]rotaxane **2·4PF$_6$** and the [2]rotaxane **3·4PF$_6$** in yields of 23 and 5%, respectively, after counterion exchange. Again, purification was achieved by column chromatography employing

(7) For examples of dumbbell-shaped two directional dendrimers, see: (a) Newkome, G. R.; Baker, G. R.; Saunders, M. J.; Russo, P. S.; Gupta, V. K.; Yao, Z.; Miller, J. E.; Bouillion, K. *J. Chem. Soc., Chem. Commun.* **1986**, 752−753. (b) Newkome, G. R.; Baker, G. R.; Arai, S.; Saunders, M. J.; Russo, P. S.; Theriot, K. J.; Moorefield, C. N.; Rogers, L. E.; Miller, J. E.; Lieux, T. R.; Murray, M. E.; Phillips, B.; Pascal, L. *J. Am. Chem. Soc.* **1990**, *112*, 8458−8465. (c) Newkome, G. R.; Moorefield, C. N.; Baker, G. R.; Behera, R. K.; Escamilla, G. H.; Saunders, M. J. *Angew. Chem., Int. Ed. Engl.* **1992**, *31*, 917−919. (d) Newkome, G. R.; Lin, X.; Yaxiong, C.; Escamilla, G. H. *J. Org. Chem.* **1993**, *58*, 3123−3129.

(8) The dioxybenzene-based macrocyclic polyethers, bis-*p*-phenylene-34-crown-10 and bis-*m*-phenylene-32-crown-10, bipyridine, and the 1,1′-dibenzyl-4,4′-bipyridinium dication, are abbreviated to **BPP34C10**, **BMP32C10**, **BP**, and **DBV**$^{2+}$, respectively. The generation-three bromide employed as the stopper is abbreviated to **[G-3]-S**, where **[G-3]** stands for generation-three and **S** for stopper. The salts bis[4-(4-pyridyl)pyridinium]-*p*-xylene bis(hexafluorophosphate) and bis{[4-(4-pyridyl)pyridinium]-*p*-xylene}-4,4'-bipyridinium tetrakis(hexafluorophosphate) are abbreviated to **[BPYPYXY][PF$_6$]$_2$** and **[BPYPYXYBIPY][PF$_6$]$_4$**, respectively. The remaining compounds—*i.e.* the polycationic rotaxanes—are indicated by numbers, followed by the counterions.

Scheme 2

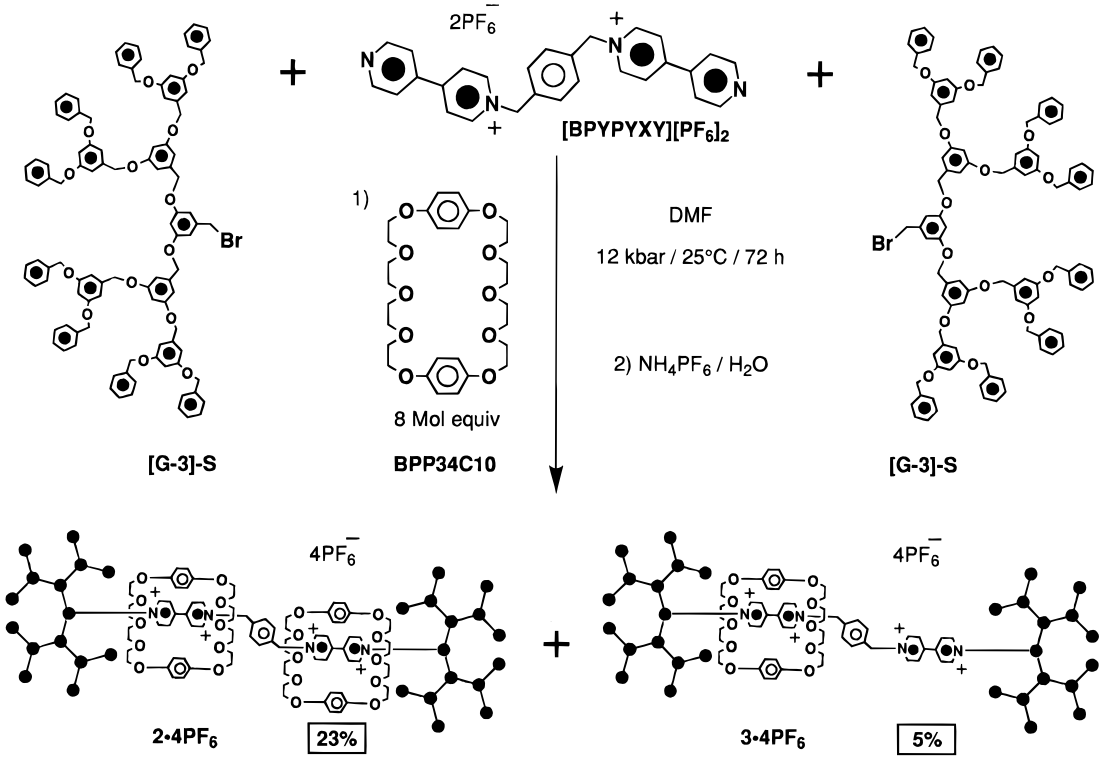

a relatively low polarity eluant despite the tetracationic nature of these rotaxanes.

Reaction (Scheme 3) of the tetrakis(hexafluorophosphate) salt **[BPYPYXYBIPY][PF$_6$]$_4$** with the stopper **[G-3]-S** in the presence of 12 molar equivalents of **BPP34C10** in DMF under ultrahigh pressure conditions at 25 °C during 72 h afforded the [4]rotaxane **4·6PF$_6$**, the [3]rotaxane **5·6PF$_6$**, and the [2]rotaxane **6·6PF$_6$** in yields of 25, 15, and 4%, respectively, after counterion exchange. Once more, purification of the resulting compounds was achieved by column chromatography employing an eluant of relatively low polarity, although each of these rotaxanes bears six positive charges! Furthermore, these hexacationic rotaxanes are highly soluble in most of the common organic solvents.

^{1}H-NMR Spectroscopy. The chemical shifts (δ) of the protons in the α- and β-positions with respect to the nitrogen atoms on the bipyridinium units incorporated within the dumbbell-shaped components, as well as the δ values for the protons attached to the hydroquinone rings incorporated within

Scheme 3

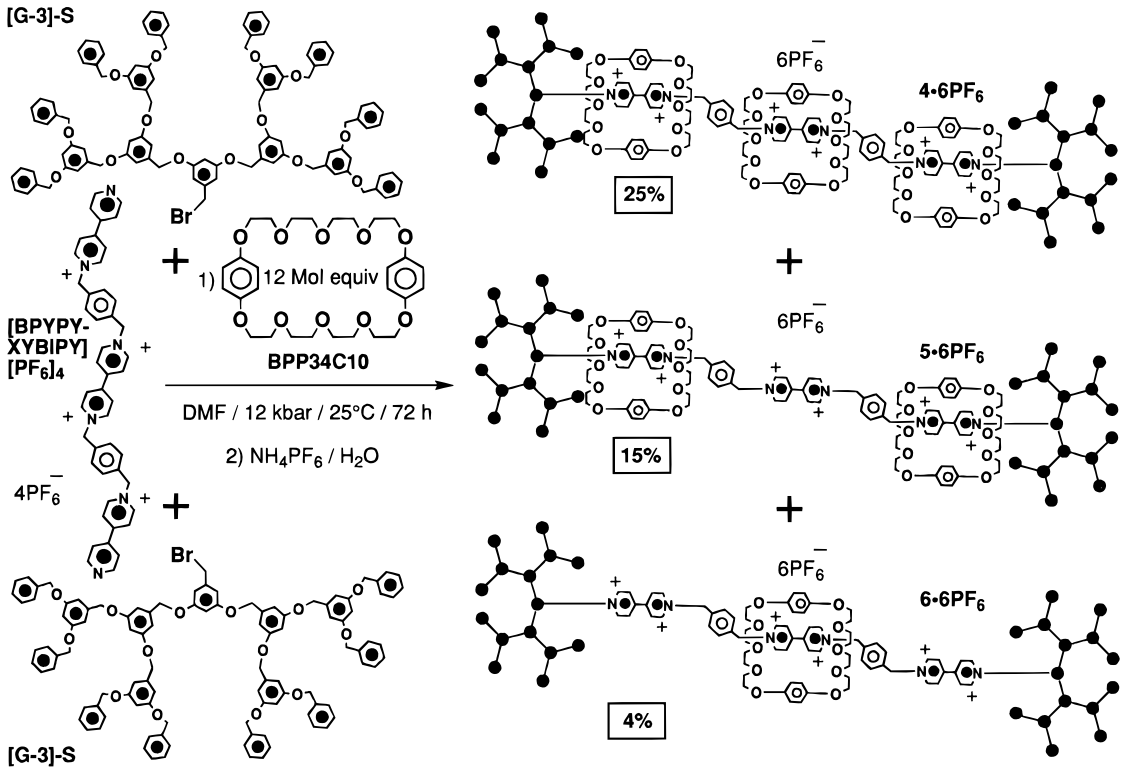

Table 1. Chemical Shifts (δ) in CD_3COCD_3 at Ambient Temperature for the Macrocyclic Polyether **BPP34C10**, the [2]Rotaxanes **1·2Br**, **3·4PF$_6$**, and **6·6PF$_6$**, the [3]Rotaxanes **2·4PF$_6$** and **5·6PF$_6$**, and the [4]Rotaxane **4·6PF$_6$**

compd	α-CH[a] (δ)	β-CH[b] (δ)	ArH[c] (δ)
BPP34C10			6.77
1·2Br[d]	9.41	8.35	6.07
2·4PF$_6$[e]	9.14	8.20	6.07
3·4PF$_6$[e]	9.26	8.41	6.05
4·6PF$_6$[e,f]	9.13	8.21	6.10, 6.06
5·6PF$_6$[e]	9.22	8.35	6.17
6·6PF$_6$[e]	9.40	8.64	6.20

[a] Chemical shifts (δ) of the protons in the α-positions with respect to the nitrogen atoms on the bipyridinium units. [b] Chemical shifts (δ) of the protons in the β-positions with respect to the nitrogen atoms on the bipyridinium units. [c] Chemical shifts (δ) of the protons attached to the hydroquinone rings incorporated within the **BPP34C10** macrocycle. [d] Broad resonances are observed for the α-protons and β-protons of the [2]rotaxane **1·2Br**. The center of these signals corresponds to the δ values reported in the Table. [e] Multiplets are observed for both the α-protons and β-protons of these rotaxanes. The δ values listed in the Table correspond to the centers of the multiplets. [f] A singlet centered on δ 6.10 is observed for the protons attached to the hydroquinone rings incorporated within the two equivalent macrocyclic components encirling each one of the bipyridinium recognition sites adjacent to the stoppers. A second singlet centered on δ 6.06 is observed for the protons attached to the hydroquinone rings incorporated within the third macrocyclic component.

the macrocyclic components, are listed in Table 1. The ^{1}H-NMR spectrum of the [2]rotaxane **1·2Br**, recorded in CD_3COCD_3 at room temperature, shows two broad resonances centered on δ 9.41 and 8.35 for the α- and β-protons, respectively. In the case of the [3]rotaxane **2·4PF$_6$** and the [2]rotaxane **3·4PF$_6$**, incorporating two bipyridinium recognition sites within their dumbbell-shaped components, two sets of heterotopic α-protons, as well as two sets of heterotopic β-protons, can be differentiated. As a result, two multiplets, composed each of two partially overlapping doublets, are observed for the α- and β-protons in both rotaxanes. However, each bipyridinium recognition site incorporated within the [3]rotaxane **2·4PF$_6$** is *sandwiched* between the two π-electron-rich hydroquinone rings of a macrocyclic component. Hence, a pronounced shielding effect is suffered by the α- and β-protons which resonate at higher fields than in the case of the [2]rotaxane **3·4PF$_6$** incorporating two bipyridinium recognition sites but only one macrocyclic component. A similar effect is observed for the rotaxanes **4·6PF$_6$**, **5·6PF$_6$**, and **6·6PF$_6$** incorporating three bipyridinium recognition sites and three, two, and one macrocyclic components, respectively. One multiplet for the α-protons and one multiplet for the β-protons are observed in the ^{1}H-NMR spectra of all three rotaxanes, although significant differences in their δ values are evident. In the case of the *fully-occupied* [4]rotaxane **4·6PF$_6$**, each bipyridinium recognition site is encircled by a π-electron-rich macrocyclic component. As a result, a pronounced shielding effect is experienced by the α- and β-protons which resonate at δ 9.13 and 8.21, respectively. On the contrary, the [3]rotaxane **5·6PF$_6$** and the [2]rotaxane **6·6PF$_6$** incorporate one and two *free* bipyridinium recognition sites, respectively, and their α- and β-protons are less shielded than those of the [4]rotaxane **4·6PF$_6$**. Thus, differences ($\Delta\delta$) of 0.27 and 0.43 ppm between signals of the α- and β-protons, respectively, of the [4]rotaxane **4·6PF$_6$** and [2]rotaxane **6·6PF$_6$** are observed. The protons attached to the hydroquinone rings of the *free* **BPP34C10** macrocycle resonate as a singlet at δ 6.77 in CD_3COCD_3 at room temperature. However, in the case of the rotaxanes **1·2Br**, **2·4PF$_6$**, and **3·4PF$_6$**, the protons attached to the hydroquinone rings of their **BPP34C10** macrocyclic components are significantly shifted upfield (*ca.* 0.7 ppm). Similarly, the ^{1}H-NMR spectra of the [3]rotaxane **5·6PF$_6$** and the [2]rotaxane **6·6PF$_6$** show singlets at δ 6.17 and 6.20, respectively, corresponding to the hydroquinone ring protons in their **BPP34C10** macrocyclic components. In the case of the [4]rotaxane **4·6PF$_6$**, a singlet at δ 6.10 corresponding to the hydroquinone ring protons of the two equivalent **BPP34C10** macrocycles residing on the bipyridinium units adjacent to the stoppers, as well as a singlet centered on δ 6.06 corresponding to the hydroquinone ring protons of the **BPP34C10** macrocycle encircling the *central* bipyridinium recognition site, are observed.

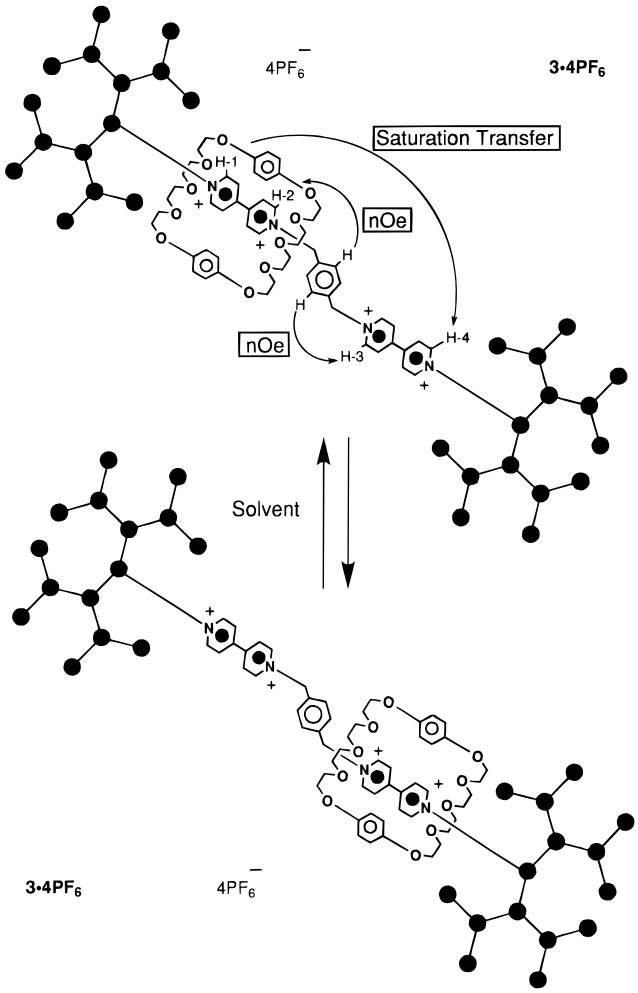

Figure 2. The degenerate site exchange process associated with the [2]rotaxane **3·4PF$_6$**.

The [2]rotaxane **3·4PF$_6$** incorporates two bipyridinium recognition sites within its dumbbell-shaped component but only one **BPP34C10** macrocyclic component. As a result, the macrocycle moves (Figure 2) back and forth from one recognition site to the other in solution, giving rise to a so-called[9] *molecular shuttle*. Variable-temperature ^{1}H-NMR spectroscopy was employed to investigate this dynamic process in some detail. At 213 K, the *shuttling* is slow on the ^{1}H-NMR time scale. Thus, the ^{1}H-NMR spectrum of **3·4PF$_6$** recorded at this temperature in CD_3COCD_3 shows (Figure 3d) four resonances for the four sets of α-protons (Figure 2). Irradiation (Figure 4) at this temperature of the protons attached to the *p*-xylene spacer separating the two bipyridinium units results in an nOe (Figure 2) experienced by the protons responsible for the resonances centered on δ 9.42 and 9.23. Furthermore, the protons attached

(9) Anelli, P. L.; Spencer, N.; Stoddart, J. F. *J. Am. Chem. Soc.* **1991**, *113*, 5131−5133.

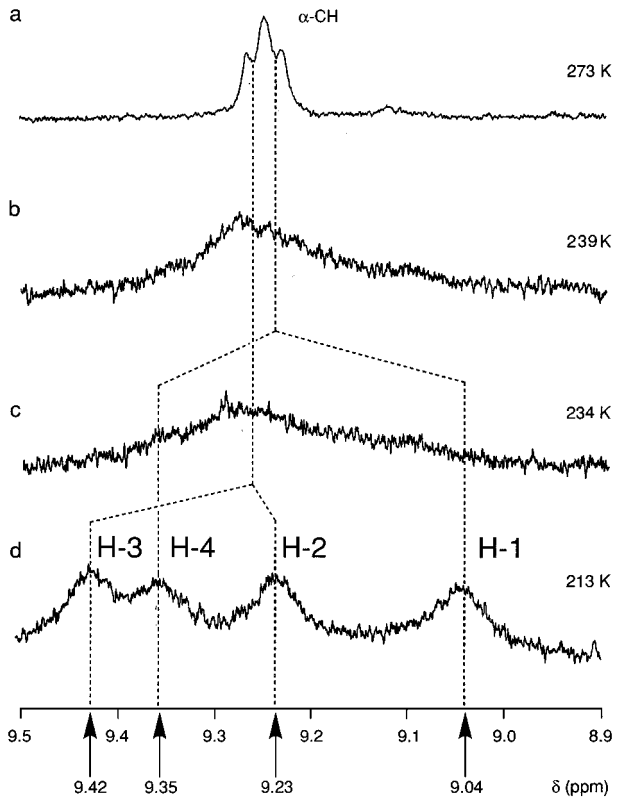

Figure 3. Partial ^{1}H-NMR spectra of the [2]rotaxane **3·4PF$_6$** recorded in CD_3COCD_3 at (a) 213, (b) 239, (c) 234, and (d) 213 K.

to *occupied* bipyridinium units resonate (*vide supra*) at higher fields than those of *unoccupied* bipyridinium recognition sites. Thus, the signals centered on δ 9.42 and 9.23 correspond to H-3 and H-2, respectively. As a result, the remaining two signals resonating at δ 9.35 and 9.04 must correspond to H-4 and H-1, respectively. Irradiation at δ 9.04 shows (Figure 5) saturation transfer to the resonance centered at δ 9.35, confirming that H-4 and H-1 are in slow exchange. As a result, coalescences of the two pairs of resonances associated with H-4 ↔ H-1 and H-3 ↔ H-2 are observed (Figures 3b and 3c, respectively) at 239 and 234 K, respectively. On warming the CD_3COCD_3 solution of **3·4PF$_6$** up to 273 K, the *shuttling* becomes fast on the ^{1}H-NMR time scale and *occupied* as well as *unoccupied* bipyridinium units, cannot be distinguished in the ^{1}H-NMR spectrum (Figure 3a) which shows only two partially-overlapped doublets. The dynamic process, associated with the [2]rotaxane **3·4PF$_6$** in solution, was investigated also in THF-d_8, CD_2Cl_2, and $CDCl_3$ by variable-temperature ^{1}H-

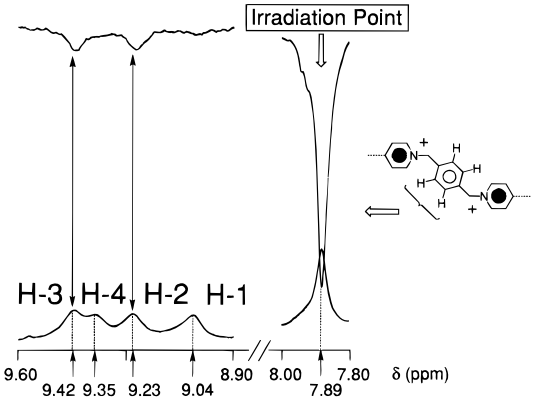

Figure 4. Partial ^{1}H-NMR spectra of the [2]rotaxane **3·4PF$_6$** recorded in CD_3COCD_3 at 213 K illustrating the nOe occurring between the protons attached to the *p*-xylene spacer and H-2 and H-3.

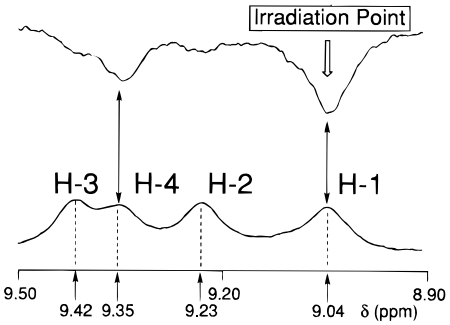

Figure 5. Partial ^{1}H-NMR spectra of the [2]rotaxane **3·4PF$_6$** recorded in CD_3COCD_3 at 213 K illustrating the saturation transfer from H-1 to H-4.

NMR spectroscopy which revealed a temperature dependence very similar to that observed in CD_3COCD_3. By employing the coalescence methodology,[10] the kinetic parameters (Table 2) associated with the degenerate site exchange process—namely the *shuttling*—were calculated for all four solvents. However, the free energies of activation reported in Table 2 were calculated at the coalescence temperatures which differ significantly in the four solvents for both probes I and II. Thus, in order to compare the energy barriers associated with the *shuttling* process, extrapolation of $\Delta G^{\ddagger}$ at the same temperature for the four solvents is required. At 298 K—*i.e.* at approximately ambient temperature—the energy of activation increases by *ca.* 3 kcal mol^{-1} on going from CD_3COCD_3 to $CDCl_3$ (from top to bottom in Table 2), corresponding to a decrease of the rate of *shuttling* of the macrocyclic component from one bipyridinium recognition site to the other from *ca.* 33000 to 200 times per second!

Molecular Modeling Studies. As a result of the amorphous nature of the dendritic rotaxanes **1**−**6** that ruled out single-crystal X-ray crystallographic analyses, we embarked on the investigation of some of the possible three-dimensional surfaces of these molecules by using the molecular modeling package[11] Macromodel 5.0. Calculations of the approximate size of the rotaxanes suggested that their end-to-end overall lengths[12] range from 30 to 60 Å (3−6 nm)—increasing by *ca.* 15 Å (1.5 nm) upon introduction of a new bipyridinium recognition site within the dumbbell-shaped component. As well as these observations, their approximate molecular volumes range from 4000 to 6000 Å^3 (4−6 nm^3). Figure 6 illustrates a space-filling representation of the [4]rotaxane **4**$^{6+}$. Molecular modeling dynamics simulations of the [2]rotaxane **3**$^{4+}$—a *molecular shuttle*—were performed in either $CHCl_3$ or Me_2CO solvent models with and without counterions. Playback of the movie files thus generated show that folding of the structure occurs in $CHCl_3$ even when the counterions are present—presumably, in order to minimize the exposure of the dicationic bipyridinium units to a relatively low polarity solvent. The resulting compressed globular structure imparts large amounts of steric and electronic hindrance upon the *shuttling* process, resulting in a significant solvent dependence of the dynamic process supporting the variable-temperature ^{1}H-NMR spectroscopic observations (*vide infra*), *i.e.* the energy of activation associated with the *shuttling* process (Table 2) is higher in $CHCl_3$ than it is in Me_2CO.

(10) (a) Sutherland, I. O. *Annu. Rep. NMR Spectrosc.* **1971**, *4*, 71−235. (b) Sandström, J. *Dynamic NMR Spectroscopy*; Academic Press: London, 1982.

(11) Mahamadi, F.; Richards, N. G. K.; Guida, W. C.; Liskamp, R.; Lipton, M.; Caufield, D.; Chang, G.; Hendrickson, T.; Still, W. C. *J. Comp. Chem.* **1990**, *11*, 440−467.

(12) The approximate end-to-end lengths of the rotaxanes were calculated as the distances between two points located in space at the most remote site of the surface of the dendritic stopper and laying on the mean plane defined by the polycationic thread.

Table 2. Kinetic Parameters[a] for the Degenerate Site Exchange Process Associated with the [2]Rotaxane **3·6PF$_6$**

	probe I[b]				probe II[c]			
solvent	$\Delta\nu$[d] (Hz)	k_c[e] (Hz)	T_c[f] (K)	$\Delta G_c^{\ddagger}$[g] (kcal mol^{-1})	$\Delta\nu$[d] (Hz)	k_c[e] (Hz)	T_c[f] (K)	$\Delta G_c^{\ddagger}$[g] (kcal mol^{-1})
CD_3COCD_3	124	276	239	11.2	76	169	234	11.2
THF-d_8	64	142	234	11.3	140	311	245	11.5
CD_2Cl_2	116	258	254	12.0	44	98	237	11.6
$CDCl_3$	140	311	299	14.1	100	222	290	13.9

[a] Two sets of data were calculated in each solvent by following two independent pairs of coalescing resonances. [b] In the case of CD_3COCD_3, CD_2Cl_2, and $CDCl_3$, probe I corresponds to the pair of coalescing resonances H-1 ↔ H-4 (Figure 2). In the case of THF-d_8, the four sets of α-protons give rise to only two coalescing resonances. The signal resonating at higher fields corresponds to the α-protons H-1 and H-2 of the *occupied* bipyridinium recognition site while the second resonance corresponds to the α-protons H-3 and H-4 attached to the *unoccupied* bipyridinium unit. This pair of coalescing resonances was employed as probe I. [c] In the case of CD_3COCD_3, CD_2Cl_2, and $CDCl_3$, probe II corresponds to the pair of coalescing resonances H-2 ↔ H-3 (Figure 2). In the case of THF-d_8, the four sets of β-protons give rise to two coalescing resonances which were employed as probe II. [d] Limit frequency separation ($\Delta\nu$) between the coalescing resonances. [e] Rate constant (k_c) at the coalescence temperature (T_c) for the degenerate site exchange process calculated from the expression $k_c = \pi(\Delta\nu)/2^{1/2}$. [f] Temperature of the spectrometer probe at coalescence. [g] Free energy barrier ($\Delta G_c^{\ddagger}$) at coalescence associated with the degenerate site exchange process calculated by employing the following equation, $\Delta G_c^{\ddagger} = [23.759 - \ln(k_c T_c^{-1})]RT_c$, where R is the gas constant.

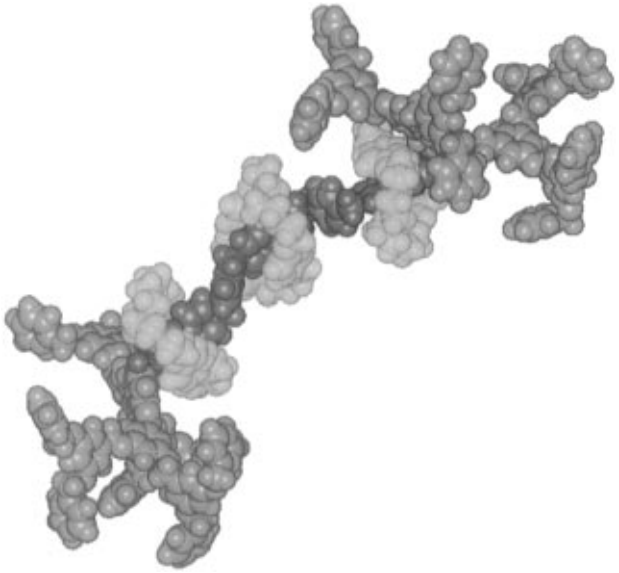

Figure 6. Computer-generated space-filling representation of the [4]-rotaxane **4**$^{6+}$.

Absorption Spectra and Luminescence Properties. The rotaxanes **1**−**6** contain several chromophoric units—namely, two dendritic stoppers, one or more bipyridinium units, and one or more **BPP34C10** macrocyclic polyethers. The absorption spectra and luminescence properties of the isolated bipyridinium units and of the macrocyclic polyether **BPP34C10** have been reported previously[13] and, in both cases, absorption bands (Table 3) above 350 nm are not observed. In addition, the bipyridinium chromophore does not show any luminescence, while **BPP34C10** exhibits a strong fluorescence band centered on 320 nm. The third generation dendritic stopper **[G-3]-S** contains several 1,3-dioxybenzene chromophores. Similarly, the macrocyclic polyether **BMP32C10** contains two 1,3-dioxybenzene chromophores and reveals two very close absorption bands (λ_{max}, 275 and 281 nm; ϵ, 3700 and 3300 M^{-1} cm^{-1}, respectively) and one emission band (λ_{max}, 300 nm; τ, 1 ns), as revealed in a previous investigation.[14] The **[G-3]-S** stopper shows (Figure 7) a relatively broad absorption band (λ_{max}, 282 nm) whose intensity (ϵ, 14 000 M^{-1} cm^{-1}) is approximately that expected according to the number of its 1,3-dimethoxybenzene chromophores. However, in contrast with **BMP32C10**, an absorption tail at lower energy is observed for **[G-3]-S**. Excitation at the maximum of the absorption band of **[G-3]-S** results in a very short-lived emission (λ_{max}, 313 nm) with a tail at lower energy. When the excitation is performed at a λ value of 310 nm, a new broad emission band (Figure 7) appears at 390 nm. The excitation spectrum at λ_{em} equal to 300 nm matches well the absorption band centered on 282 nm, whereas the excitation spectrum at λ_{em} equal to 390 nm shows a broad band with maximum (310 nm) in the region of the absorption tail. Moreover, the emission band with the λ_{max} of 313 nm is about 10 times weaker than that (λ_{max}, 305 nm) of **BMP32C10**. These results indicate that in the **[G-3]-S** stopper, some of the 1,3-dimethoxybenzene chromophores undergo noticeable ground and excited state interactions.

In the [2]rotaxane **1·2Br**, the [3]rotaxane **2·4PF$_6$**, and the [4]rotaxane **4·6PF$_6$**, the absorption spectrum in the UV region resembles closely the sum of the absorption spectra of the components—namely, the dendritic stoppers, the bipyridinium units, and the macrocyclic polyethers. In the visible region, the characteristic[13] charge-transfer absorption band (Figure 8) arising from donor−acceptor interactions between the bipyridinium units and the hydroquinone ring incorporated within the macrocyclic polyethers is observed. The intensity of the charge-transfer band is approximately proportional to the number of bipyridinium units encircled by the macrocyclic polyethers. The maximum of the absorption band and the contribution of each threaded unit to the molar absorption coefficient are virtually the same as in analogous [*n*]rotaxanes incorporating tetraarylmethane-based stoppers.[1]

The [2]rotaxane **1·2Br**, the [3]rotaxane **2·4PF$_6$**, and the [4]-rotaxane **4·6PF$_6$** exhibit a weak emission band with a maximum at *ca*. 320 nm. This emission shows the same excitation spectrum and lifetime as in the case of **BPP34C10**, but it is about 50 times weaker. We assign this residual emission to the presence of small amounts of hydroquinone-containing impurities. As a result, we can conclude that the luminescence exhibited by **[G-3]-S** and **BPP34C10** is quenched within the rotaxanes by the low energy levels originating from the charge-transfer interactions between the bipyridinium units and the hydroquinone-based macrocyclic polyethers, consistent with the rotaxanes and catenanes containing π-electron-donor and π-electron-acceptor units which have been investigated so far.

Electrochemical Properties. The electrochemical data associated with the macrocyclic polyether **BPP34C10**,[13] the 1,1′-dibenzyl-4,4′-bipyridinium dication **DBV**$^{2+}$, the third generation stopper **[G-3]-S**, the [2]rotaxane **1·2Br**, the [3]rotaxane **2·4PF$_6$**,

(13) Anelli, P. L.; Ashton, P. R.; Ballardini, R.; Balzani, V.; Delgado, M.; Gandolfi, M. T.; Goodnow, T. T.; Kaifer, A. E.; Philp, D.; Pietraszkiewicz, M.; Prodi, L.; Reddington, M. V.; Slawin, A. M. Z.; Spencer, N.; Stoddart, J. F.; Vicent, C.; Williams, D. J. *J. Am. Chem. Soc.* **1992**, *114*, 193−218.

(14) Ballardini, R.; Gandolfi, M. T.; Prodi, L.; Ciano, M.; Balzani, V.; Kohnke, F. H.; Shahriari-Zavareh, H.; Spencer, N.; Stoddart, J. F. *J. Am. Chem. Soc.* **1989**, *111*, 7052−7078.

Table 3. Absorption, Luminescence, and Electrochemical Data of the [2]Rotaxane **1·Br**, the [3]Rotaxane **2·4PF$_6$**, the [4]Rotaxane **4·6PF$_6$**, and their Components in MeCN at Room Temperature

	absorption[a]		luminescence[a]			electrochemistry[b]	
compd	λ_{max} (nm)	ϵ_{max} (M^{-1} cm^{-1})	λ_{max} (nm)	Φ_{em}	τ (ns)	reduction$E_{1/2\,[n]}$[c] (V *vs* SCE)	oxidationE^{d} (V *vs* SCE)
[G-3]-S	282	14000	313[e]	4×10^{-3}	< 1		+1.6
			390[f]	7×10^{-3}	8.5		
DBV^{2+}	259	18000				−0.35 [1]	
						−0.78 [1]	
BPP34C10[g]	290	5200	320	0.11	2.6		+1.3
1·2Br	278	44000				−0.44 [1]	+1.4
	457	580[h]					+1.6
2·4PF$_6$	277	60000				−0.44 [2]	+1.4
	457	1000					+1.6
4•6PF$_6$	275	77000				−0.43 [3]	+1.4
	457	1450					+1.6

[a] Air-equilibrated solution. [b] Argon-purged solution. [c] The number of exchanged electrons *n* is indicated in square brackets. [d] Irreversible process; values estimated from DPV peaks. [e] Excitation wavelength 270 nm. [f] Excitation wavelength 310 nm. [g] Literature values (Anelli, P. L.; Ashton, P. R.; Ballardini, R.; Balzani, V.; Delgado, M.; Gandolfi, M. T.; Goodnow, T. T.; Kaifer, A. E.; Philp, D.; Pietraszkiewicz, M.; Prodi, L.; Reddington, M. V.; Slawin, A. M. Z.; Spencer, N.; Stoddart, J. F.; Vicent, C.; Williams, D. J. *J. Am. Chem. Soc.* **1992**, *114*, 193−218.). [h] Red-side shoulder of a very intense UV band.

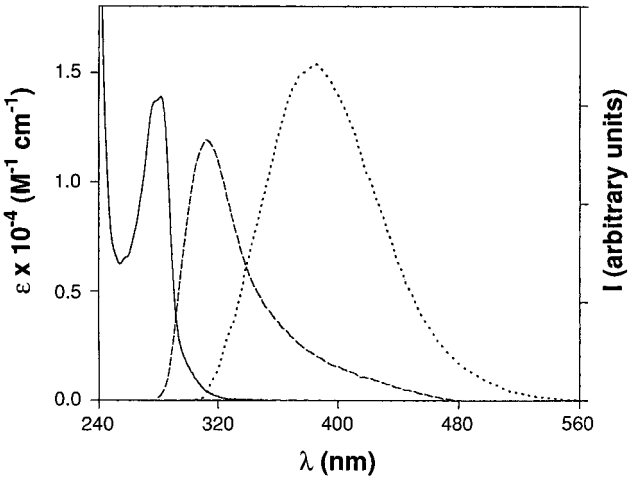

Figure 7. Absorption (full line) and fluorescence (λ_{ex}, 270 nm, dashed line; λ_{ex}, 310 nm, dotted line) spectra of **[G-3]-S**.

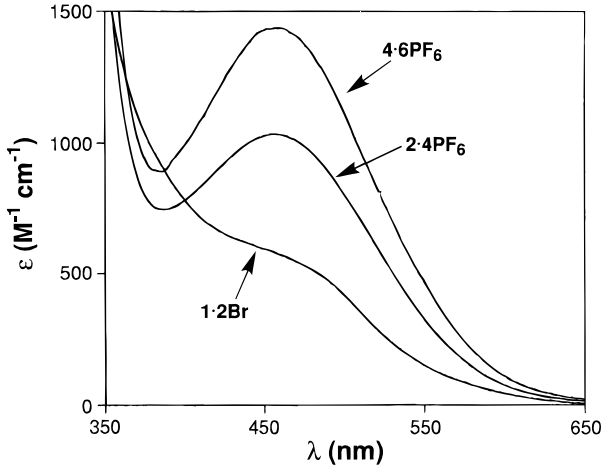

Figure 8. Charge-transfer absorption bands in the visible region of the [2]rotaxane **1·2Br**, the [3]rotaxane **2·4PF$_6$**, and the [4]rotaxane **4·6PF$_6$** in MeCN solution at room temperature.

and the [4]rotaxane **4·6PF$_6$** are all listed in Table 3. As far as the reduction processes are concerned, they involve only the bipyridinium units. **DBV^{2+}** (which can be taken as a model compound for the examined [*n*]rotaxanes) shows two reversible one-electron reduction processes, according to the behavior exhibited by the well known 1,1′-dimethyl-4,4′-bipyridinium dication. These reductions occur at less negative potential (about 80 mV) with respect to the 1,1′-dimethyl-4,4′-bipyridinium dication, as expected for the replacement of methyl groups with the electron accepting benzyl groups on the *N*-positions. In the [*n*]rotaxanes, the only process that could be studied with accuracy was the first reversible reduction of the bipyridinium units. Electrode adsorption, presumably as a result of the presence of the dendritic stoppers, prevented us from obtaining accurate current intensity and potential values for the second reduction of the bipyridinium units. The results obtained show that *(i)* the reduction of bipyridinium units encircled by the **BPP34C10** macrocyclic polyether occurs at more negative potentials than the reduction of **DBV^{2+}**; *(ii)* in the [*n*]rotaxanes containing more than one bipyridinium unit, reduction of such units occurs at the same potential and the current intensities of the cyclic voltammograms (as well as the peak areas of the differential pulse voltammetry) increase linearly with the number of units; and *(iii)* the reduction potential is substantially the same for the three [*n*]rotaxanes investigated. The shift toward more negative potentials for the reduction of the bipyridinium units threaded through the cavity of **BPP34C10** is the expected consequence of the charge-transfer interactions with the hydroquinone rings incorporated within the macrocyclic polyether. Reduction of the two chemically-equivalent bipyridinium units of **2·4PF$_6$** at the same potential was also expected because of the lack of substantial electronic interaction which has been observed previously in other [*n*]rotaxanes, as well as in their dumbbell-shaped components.[1a] However, the fact that in **4·6PF$_6$** the three bipyridinium units are reduced at the same potential is somewhat surprising since the central bipyridinium unit is not equivalent to the lateral ones. Also, it is known that the reduction potential of the bipyridinium units is very sensitive to the nature of the substituents on the nitrogen.[1a] For the same reason, it is surprising that reduction of the bipyridinium units of **1·2Br**, **2·4PF$_6$**, and **4·6PF$_6$** occurs at almost the same potential. In particular, for rotaxanes analogous to **1·2Br** and **2·4PF$_6$**, but not bearing dendritic stoppers, we have found a difference of 30 mV in the reduction potential.[1a] This observation suggests that the dendritic nature of the stoppers plays a role in determining the electrochemical behavior of these rotaxanes. A more detailed analysis of this effect would require the examination of the presently unavailable dumbbell-shaped components of the examined [*n*]rotaxanes.

The oxidation processes observed in the [*n*]rotaxanes, involving the dioxybenzene units of the stoppers and of **BPP34C10**, are not fully reversible. However, some considerations follow from comparing the behavior of **[G-3]-S** with that of the previously studied[13] **BPP34C10** macrocycle. In the case of

[G-3]-S, a very intense differential pulse voltammetry peak was observed at +1.6 V. This peak is very broad, indicating non-negligible electronic interactions among the dimethoxybenzene units. In the [*n*]rotaxanes, at least two processes are observed. The first one (+1.4 V) can be assigned to oxidation of the **BPP34C10** macrocyclic polyethers engaged in charge-transfer interaction.[13] The second process can be assigned to the dendritic stoppers, since it occurs at the same potential as the oxidation of **[G-3]-S**.

Conclusions

We have combined the convergent approach to dendritic nanostructures with the threading approach to self-assembling rotaxanes in order to generate six novel [*n*]rotaxanes. These molecular structures incorporate a bipyridinium-based rotaxane-like core embedded within a dendritic framework. The properties associated with the polycationic rotaxane-like cores are dramatically influenced by the dendritic shell present around them. Thus, the highly-charged rotaxanes are easily soluble in most common organic solvents. As a result, the solvent dependence of the dynamic process—namely the *shuttling* action—involving the movement of the macrocyclic component along the dumbbell-shaped component of one of these rotaxanes could be investigated for the first time. The dramatic solvent dependence of the rate of the process—the rate increases with the polarity of the medium—is a result of conformational changes induced by varying the solvent polarity, as suggested by molecular dynamics simulations. These computational studies have allowed us to visualize also the three-dimensional structures of such nanoscopic-sized molecular assemblies composed of a functioning rotaxane-like core embedded within a dendritic framework.

Experimental Section

General Methods. Chemicals were purchased from Aldrich and used as received. DMF was dried from CaH_2 according to literature procedures.[15] The macrocyclic polyether **BPP34C10**,[13] the hexafluorophosphate salts **[BPYPYXY][PF$_6$]$_2$**[13] and **[BPYPYXYBIPY][PF$_6$]$_4$**,[1a] as well as the third generation bromide **[G-3]-S**[16] were prepared according to literature procedures. Reactions were carried out in Teflon vessels using a custom-built ultrahigh pressure reactor manufactured by PSIKA Pressure Systems Limited of Glossop, UK. Thin-layer chromatography (TLC) was carried out on aluminium sheets coated with silica-gel 60 (Merck 5554). Column chromatography was performed on silica-gel 60 (Merck 9385, 230−400 mesh). Melting points were determined on an Electrothermal 9200 melting point apparatus and are uncorrected. Liquid secondary ion mass spectra (LSIMS) were obtained from a VG Zabspec mass spectrometer, equipped with a 35 keV cesium ion gun. Samples were dissolved in either a 3-nitrobenzyl alcohol or 2-nitrophenyl octyl ether matrix previously coated on to a stainless steel probe tip. High-resolution accurate mass measurements were obtained from the Zabspec by employing narrow voltage scanning at a resolution of *ca.* 10.000 and employing a cesium/rubidium iodide reference. Electrospray positive-ion mass spectra (ESMS) were measured on a VG Prospec mass spectrometer. ^{1}H-NMR spectra were recorded on a Bruker AC300 (300 MHz) or a Bruker AMX400 (400 MHz) spectrometer. ^{13}C-NMR spectra were recorded on a Bruker AC300 (75 MHz) spectrometer.

[2]Rotaxane 1·2Br. A DMF (5 mL) solution of **BP** (4.0 mg, 0.03 mmol), the bromide **[G-3]-S** (100.0 mg, 0.06 mmol), and the macrocycle **BPP34C10** (56.0 mg, 0.10 mmol) was subjected to a pressure of 12 kbar during 72 h at 25 °C. The solvent was removed in *vacuo* and the resulting red oil was purified by column chromatography (SiO_2, CH_2Cl_2/EtOH, 9.5:0.5) to yield the [2]rotaxane **1·2Br** (28.5 mg, 27%) as a red glassy solid: LSIMS, *m/z* 3845 [M − 2Br]$^+$; HRMS (LSIMS) calcd for [M − 2Br]$^+$ $C_{246}{}^{13}C_2H_{230}N_2O_{38}$ 3845.6196, found 3845.6219; ESMS, *m/z* 1923 [M − 2Br]$^{2+}$; ^{1}H-NMR (CD_3COCD_3) δ 9.45−9.36 (4H, m), 8.40−8.30 (4H, m), 7.38−7.20 (80H, m), 6.78−6.63 (28H, m), 6.61−6.50 (14H, m), 6.13−6.01 (12H, m), 5.10 (8H, s), 5.00 (16H, s), 4.92 (32H, s), 3.63−3.46 (32H, m); ^{13}C-NMR ($CDCl_3$) δ 168.4, 160.9, 160.1, 160.0, 151.8, 146.0, 144.5, 139.1, 138.8, 136.7, 134.5, 128.5, 128.0, 127.5, 126.3, 116.1, 108.9, 106.4, 103.6, 101.6, 101.5, 70.3, 70.0, 69.9, 67.6, 64.0. Anal. Calcd for $C_{248}H_{230}Br_2N_2O_{38}\cdot 2H_2O$: C, 73.36; H, 5.86; N, 0.69. Found: C, 73.21; H, 5.50; N, 0.98.

[3]Rotaxane 2·4PF$_6$ and [2]Rotaxane 3·4PF$_6$. A DMF (5 mL) solution of the bis(hexafluorophosphate) salt **[BPYPYXY][PF$_6$]$_2$** (18.0 mg, 0.03 mmol), the bromide **[G-3]-S** (100.0 mg, 0.06 mmol), and the macrocycle **BPP34C10** (112.0 mg, 0.21 mmol) was subjected to a pressure of 12 kbar during 72 h at 25 °C. The solvent was removed in *vacuo* and the resulting red oil was purified by column chromatography (SiO_2, CH_2Cl_2/Me_2CO/EtOH, 9.5:0.25:0.25) to yield a red glassy solid. The solid was dissolved in a saturated Me_2CO solution (30 mL) of NH_4PF_6 and the resulting solution was stirred at room temperature for 1 h. The solvent was removed in *vacuo* and the residue washed with H_2O (50 mL) to afford the [3]rotaxane **2·4PF$_6$** (31.0 mg, 23%) as a red glassy solid. The column was then eluted with CH_2Cl_2/EtOH (9.5:0.5) to afford a red glassy solid which was subjected to counterion exchange (NH_4PF_6/Me_2CO and then H_2O, as described for **2·4PF$_6$**) to yield the [2]rotaxane **3·4PF$_6$** (6.2 mg, 5%). **2·4PF$_6$**: LSIMS: *m/z* 5078 [M − PF$_6$]$^+$, 4932 [M − 2PF$_6$]$^+$; HRMS (LSIMS) calcd for [M − 2PF$_6$]$^+$ $C_{291}{}^{13}C_3H_{286}F_{12}N_4O_{48}P_2$ 4932.9446, found 4932.9329; ESMS, *m/z* 2467 [M − 2PF$_6$]$^{2+}$, 1596 [M − 3PF$_6$]$^{3+}$, 1161 [M − 4PF$_6$]$^{4+}$; ^{1}H-NMR (CD_3COCD_3) δ 9.18−9.10 (8H, m), 8.24−8.16 (8H, m), 7.96 (4H, s), 7.46−7.26 (80H, m), 7.02−7.00 (4H, m), 6.86−6.83 (2H, m), 6.72−6.65 (24H, m), 6.64−6.58 (12H, m), 6.20 (4H, s), 6.07 (16H, s), 6.01 (4H, s), 5.11 (8H, s), 5.05 (32H, s), 4.94 (16H, s), 3.72−3.56 (64H, m); ^{13}C-NMR ($CDCl_3$) δ 167.4, 161.4, 160.8, 160.8, 152.7, 147.0, 146.8, 146.5, 146.3, 140.3, 140.0, 137.9, 136.2, 135.8, 131.5, 129.1, 128.5, 128.2, 125.9, 125.8, 116.0, 115.4, 109.5, 107.1, 101.8, 101.7, 71.2, 71.1, 71.0, 70.8, 70.5, 70.3, 70.1, 68.7, 68.1. Anal. Calcd for $C_{294}H_{286}F_{24}N_4O_{48}P_4$: C, 67.60; H, 5.52; N, 1.07. Found: C, 67.73; H, 5.60; N, 0.97. **3·4PF$_6$**: LSIMS, *m/z* 4540 [M − PF$_6$]$^+$, 4395 [M − 2PF$_6$]$^+$, 4250 [M − 3PF$_6$]$^+$; HRMS *m/z* (LSIMS) Calcd for [M − 2PF$_6$]$^+$ $C_{264}{}^{13}C_2H_{246}F_{12}N_4O_{38}P_2$ 4395.6791, found 4395.6718; ESMS, *m/z* 2198 [M − 2PF$_6$]$^{2+}$, 1417 [M − 3PF$_6$]$^{3+}$, 1027 [M − 4PF$_6$]$^{4+}$; ^{1}H-NMR (CD_3COCD_3) δ 9.30−9.32 (8H, m), 8.45−8.36 (8H, m), 7.87 (4H, s), 7.46−7.26 (80H, m), 6.96−6.93 (4H, m), 6.83−6.81 (2H, m), 6.73−6.67 (24H, m), 6.65−6.60 (12H, m), 6.16 (4H, s), 6.05 (8H, s), 5.97 (4H, s), 5.09−5.03 (40H, m), 4.97 (16H, s), 3.73−3.53 (32H, m); ^{13}C-NMR ($CDCl_3$) δ 169.3, 167.6, 166.7, 165.4, 161.4, 160.9, 160.8, 152.8, 146.5, 146.4, 146.3, 140.3, 140.0, 137.9, 135.9, 131.4, 129.1, 128.5, 128.3, 127.1, 126.9, 115.4, 109.4, 107.141, 101.8, 101.7, 71.1; 70.8, 70.8, 70.5, 70.3, 70.2, 70.1, 69.9, 68.1.

[4]Rotaxane 4·6PF$_6$, [3]Rotaxane 5·6PF$_6$, and [2]Rotaxane 6·6PF$_6$. A DMF (10 mL) solution of the tetrakis(hexafluorophosphate) salt **[BPYPYXYBIPY][PF$_6$]$_4$** (66.0 mg, 0.05 mmol), the bromide **[G-3]-S** (200.0 mg, 0.12 mmol), and the macrocycle **BPP34C10** (334.0 mg, 0.31 mmol) was subjected to a pressure of 12 kbar during 72 h at 25 °C. The solvent was removed in *vacuo* and the resulting red oil was purified by column chromatography (SiO_2, CH_2Cl_2/EtOH, 9.5:0.5) to yield three red glassy solids. The solids were dissolved separately in saturated Me_2CO solutions (30 mL) of NH_4PF_6 and the resulting solution were stirred at room temperature for 1 h. The solvents were removed in *vacuo* and the residues washed with H_2O (50 mL) to afford, in order of elution, the [4]rotaxane **4·6PF$_6$** (83.2 mg, 25%), the [3]-rotaxane **5·6PF$_6$** (45.0 mg, 15%), and the [2]rotaxane **6·6PF$_6$** (9.8 mg, 4%) as red glassy solids. **4·6PF$_6$**: LSIMS, *m/z* 6165 [M − PF$_6$]$^+$, 6019 [M − 2PF$_6$]$^+$, 5874 [M − 3PF$_6$]$^+$; HRMS, *m/z* (LSIMS) Calcd for [M − PF$_6$]$^+$ $C_{337}{}^{13}C_3H_{342}F_{30}N_6O_{58}P_5$ 6306.2306, found 6306.2366; ESMS, *m/z* 1958 [M − 3PF$_6$]$^{3+}$, 1433 [M − 4PF$_6$]$^{4+}$, 1117 [M − 5PF$_6$]$^{5+}$; ^{1}H-NMR (CD_3COCD_3) δ 9.19−9.08 (12H, m), 8.25−8.16 (12H, m), 7.96 (8H, s), 7.47−7.27 (80H, m), 7.04−7.01 (4H, m), 6.88−6.84 (2H, m), 6.74−6.66 (24H, m), 6.65−6.59 (12H, m), 6.20 (8H, s), 6.10 (16H, s), 6.06 (8H, s), 6.01 (4H, s), 5.12 (8H, s), 5.06 (32H, s), 4.96 (16H, s), 3.74−3.57 (96H, m); ^{13}C-NMR (CD_3COCD_3) δ 166.7, 161.4, 160.8, 160.8, 152.7, 152.7, 147.0, 146.8, 146.5, 146.4, 140.3,

(15) Furniss, B. S.; Hannaford, A. J.; Smith, P. W. G.; Tatchell, A. R. *Practical Organic Chemistry*; Longman: New York, 1989.
(16) Hawker, C. J.; Fréchet, J. M. J. *J. Am. Chem. Soc.* **1990**, *112*, 7638−7647.

140.1, 137.9, 136.2, 135.8, 131.5, 129.1, 128.5, 128.2, 125.9, 115.4, 109.5, 107.0, 106.7, 106.6, 103.7, 101.9, 101.7, 71.0, 70.8, 70.5, 70.3, 70.1, 69.7, 68.1, 64.9, 64.3. Anal. Calcd for $C_{340}H_{342}F_{36}N_6O_{58}P_6$: C, 64.72; H, 5.46; N, 1.33. Found: C, 64.78; H, 5.51; N, 1.23. **5·6PF$_6$**: LSIMS, *m/z* 5628 $[M - PF_6]^+$, 5483 $[M - 2PF_6]^+$, 5335 $[M - 3PF_6]^+$; ESMS, *m/z* 2744 $[M - 2PF_6]^{2+}$, 1780 $[M - 3PF_6]^{3+}$,1298 $[M - 4PF_6]^{4+}$, 1010 $[M - 5PF_6]^{5+}$; ^{1}H-NMR (CD_3COCD_3) δ 9.26−9.17 (12H, m), 8.40−8.29 (12H, m), 7.89 (8H, s), 7.40−7.26 (80H, m), 7.00−6.97 (4H, m), 6.83−6.80 (2H, m), 6.73−6.67 (24H, m), 6.64−6.59 (12H, m), 6.17 (8H, s), 6.08 (16H, s), 5.99 (4H, s), 5.09 (8H, s), 5.06 (32H, s), 4.97 (16H, s), 3.74−3.60 (64H, m); ^{13}C-NMR (CD_3COCD_3) δ 161.7, 161.1, 161.0, 153.0, 146.7, 146.6, 140.6, 140.3, 138.2, 135.9, 131.6, 131.6, 130.5, 129.9, 129.7, 129.3, 129.0, 128.7, 128.5, 127.0, 126.9, 116.3, 115.8, 109.7, 107.4, 104.0, 102.2, 102.0, 71.3, 71.1, 70.8, 70.6, 70.4, 68.4, 65.4, 65.0, 64.8, 55.5. Anal. Calcd for $C_{312}H_{302}F_{36}N_6O_{48}P_6 \cdot 3H_2O$: C, 64.30; H, 5.33; N, 1.44. Found: C, 64.20; H, 5.19; N, 1.34. **6·6PF$_6$**: LSIMS, *m/z* 5092 $[M - PF_6]^+$; ESMS, *m/z* 2474 $[M - 2PF_6]^{2+}$, 1601 $[M - 3PF_6]^{3+}$, 1164 $[M - 4PF_6]^{4+}$, 903 $[M - 5PF_6]^{5+}$; ^{1}H-NMR (CD_3COCD_3) δ 9.43−9.36 (12H, m), 8.69−8.58 (12H, m), 7.93 (8H, s), 7.55−7.37 (80H, m), 7.06-7.03 (4H, m), 6.91−6.88 (2H, m), 6.83−6.77 (24H, m), 6.75−6.71 (12H, m), 6.27−6.25 (8H, m), 6.20 (8H, s), 6.08 (4H, s), 5.75 (40H, s), 5.10 (16H, s), 3.75−3.58 (32H, m).

Molecular Modeling. The coordinates of the crown ether macrocycle, **BPP34C10**, were obtained from the CDS database[17] and used without any modification. The dendritic stoppers and the bipyridinium-based threads were generated separately in Macromodel 5.0.[11] The dendritic stoppers were minimized using the MM3* forcefield as implemented in Macromodel 5.0. The macrocycles were manually placed on to the threads and then the preminimized stoppers attached at both ends of the threads. Two sets of calculations—one without and the other with the inclusion of acetate counterions[18]—were carried out. The assembled rotaxanes were minimized by employing the Amber* forcefield using the Polak Ribiere conjugate gradient (PRCG) algorithm with the default extended cut-offs as resident within Macromodel 5.0. Solvation was included in the form of the GB/SA solvation model[19] for $CHCl_3$ or the appropiate dielectric value (set to distance dependent) for $CHCl_3$ (4.7) or Me_2CO (21). Molecular dynamics (timestep 1.5 fs for times of 10 and 100 ps at temperatures of 300 and 500 K) afforded structures which were extensively minimized (AMBER, PRCG, extended cut-offs, GB/SA solvation for $CHCl_3$ or a distance dependent dielectric for $CHCl_3$ and Me_2CO) until the RMS deviation was <0.5 kcal Å^{-1}. The approximate molecular volumes were calculated by employing Quanta[20] software running on a Silicon Graphics Indigo XS24 workstation.

Absorption and Luminescence Measurements. Room temperature experiments were carried out in 5×10^{-5} M MeCN solutions. Electronic absorption spectra were recorded with a Perkin-Elmer λ6 spectrophotometer. Emission spectra were obtained with a Perkin-Elmer LS50 spectrofluorimeter. Fluorescence quantum yields were determined using naphthalene in degassed cyclohexane as a standard ($\Phi = 0.23$).[21] Nanosecond lifetime measurements were performed with previously described Edinburgh single-photon counting equipment.[22] Experimental errors: absorption maxima, ±2 nm; emission maxima, ±2 nm; excited state lifetimes, ±10%; fluorescence quantum yields, ±20%.

Electrochemical Measurements. Electrochemical experiments were carried out in argon-purged MeCN solutions with a Princeton Applied Research 273 multipurpose instrument interfaced to a personal computer, using cyclic voltammetry (CV) and differential pulse voltammetry (DPV) techniques. The working electrode was a glassy carbon electrode (0.08 cm^2, Amel); its surface was routinely polished with a 0.05 μm alumina−water slurry on a felt surface immediately prior to use. The counter electrode was a Pt wire and the reference electrode was a saturated calomel electrode (SCE) separated with a fine glass frit. The concentration of the examined compounds was about 5.0×10^{-4} M; 0.05 M tetraethylammonium hexafluorophosphate was added as supporting electrolyte. Cyclic voltammograms were obtained at sweep rates of 20, 50, 200, 500, and 1000 mV s^{-1}; DPV experiments were performed with a scan rate of 20 mV s^{-1}, a pulse height of 75 mV, and a duration of 40 ms. For reversible processes the $E_{1/2}$ values are reported; the same values are obtained from the DPV peaks and from an average of the cathodic and anodic cyclic voltammetric peaks. For the oxidation processes, that are not fully reversible, the reported potential values are those evaluated from the DPV peaks. Both CV and DPV techniques have been used to measure the number of the exchanged electrons in each redox process; since the results obtained for non-reversible processes can be unreliable, no quantitative conclusions have been drawn on the number of electrons exchanged in the oxidation processes. To establish the reversibility of a process, we used the criteria of *(i)* separation of 60 mV between cathodic and anodic peaks, *(ii)* close to unity ratio of the intensities of the cathodic and anodic currents, and *(iii)* constancy of the peak potential on changing sweep rate in the cyclic voltammograms. The experimental error on the half-wave potential values was estimated to be ±20 mV.

Acknowledgment. This research was supported by the Engineering and Physical Sciences Research Council and by the European Community Human Capital and Mobility Programme in the UK, the National Science Foundation (DMR-9641291) in the USA, and the University of Bologna (Special Funds) and the Italian MURST and CNR (Progetto Strategico Tecnologie Chimiche Innovative) in Italy.

Supporting Information Available: Computer-generated space-filling representations of the [2]rotaxane **1**$^{2+}$ and of the [3]rotaxane **2**$^{4+}$ (2 pages). See any current masthead page for ordering and Internet access instructions.

JA962113H

(17) We wish to acknowledge the use of the EPSRC's Chemical Database Service at Daresbury. The United Kingdom Chemical Database Service: Fletcher, D. A., McMeeking, R. F., Parkin, D. *J. Chem. Inf. Comput. Sci.* **1996**, *36*, 746−749. 3D Search and Research using Camdridge Structural Database: Allen, F. H., Kennard, O. *Chem. Design Automation News* **1993**, *8(1)*, 1, 31−37.

(18) As a result of the poor parametrization of the hexafluorophosphate counterions within the Amber* forcefield resident in Macromodel 5.0, acetate counterions were used instead.

(19) Still, W. C.; Tempczyk, A.; Hawley, R. C.; Hendrckson, T. *J. Am. Chem. Soc.* **1990**, *112*, 6127−6129.

(20) Polygen Corporation, 200 Fifth Avenue, Waltham, MA 02254.

(21) Berlman, I. B. *Handbook of Fluorescence Spectra of Aromatic Compounds*; Academic Press: London, 1965.

(22) Armaroli, N.; Balzani, V.; Barigelletti, F.; De Cola, L.; Flamigni, L.; Sauvage, J.-P.; Hemmert, C. *J. Am. Chem. Soc.* **1994**, *116*, 5211−5217.